Jones Polynomial and Knot Transitions in Hermitian and non-Hermitian Topological Semimetals

Zhesen Yang[1,2] Ching-Kai Chiu,[3,*] Chen Fang,[1,†] and Jiangping Hu[1,3,4,‡]

[1]*Beijing National Laboratory for Condensed Matter Physics, and Institute of Physics, Chinese Academy of Sciences, Beijing 100190, China*
[2]*University of Chinese Academy of Sciences, Beijing 100049, China*
[3]*Kavli Institute for Theoretical Sciences and CAS Center for Excellence in Topological Quantum Computation, University of Chinese Academy of Sciences, Beijing 100190, China*
[4]*South Bay Interdisciplinary Science Center, Dongguan, Guangdong Province, China*

Topological nodal line semimetals host stable chained, linked, or knotted line degeneracies in momentum space protected by symmetries. In this Letter, we use the Jones polynomial as a general topological invariant to capture the global knot topology of the oriented nodal lines. We show that every possible change in Jones polynomial is attributed to the local evolutions around every point where two nodal lines touch. As an application of our theory, we show that nodal chain semimetals with four touching points can evolve to a Hopf link. We extend our theory to 3D non-Hermitian multiband exceptional line semimetals. Our work provides a recipe to understand the transition of the knot topology for protected nodal lines.

Introduction.—Topological phases of matter have been attracting extensive attention in the field of condensed matter physics [1–6]. Although the topological invariants of gapped phases are defined globally, they can be locally analyzed by studying the low energy theories of some gapless points in the Brillouin zone (BZ) from a critical phase [7,8]. For example, the Chern number can be calculated by analyzing the mass terms around all the Dirac points [7,9]. In this sense, all the gapped phases can be generated from those critical gapless phases by adding different types of perturbations [4,10].

The topological nodal line semimetals preserving chiral symmetry or space-time inversion symmetry can host stable one-dimensional (1D) degeneracy lines in the 3D BZ [6]. These nodal lines can form loops [11–20], chains [21–35], links [36–44], or knots [44,45]. Their topological properties are not only captured by the local charge [6] but also described by the global knot invariant [42,46–49]. Two nodal knot semimetals (hereafter, *knot* refers to both *link* and *knot*) belong to the same (topological equivalence) classes, if their nodal lines can be deformed to each other by nonbroken bending and stretching without crossing each other [50]. Being analogous to a Dirac point as a topo-logical phase transition, a touching point (TP), where two nodal lines touch together, might be a knot transition between two distinct knot classes. If we start from this critical phase, by adding different types of symmetry allowed perturbations, as the TPs are removed, different trivial and nontrivial nodal knot semimetals can be gen-erated, which are dubbed as *generated phases*. A question

naturally arises whether the knot topology of the nodal lines can be characterized by analyzing the local evolutions around TPs. The answer to this question provides a guide to analyze the possible generated phases emerging from nodal chain semimetals [21–35], which are symmetry protected critical phases with multiple TPs.

In this Letter, we first show that the Jones polynomial [50–52] can faithfully characterize the nodal knot semimetals protected by chiral symmetry. Similar to the transition of Chern insulator, we also show that the transition of Jones
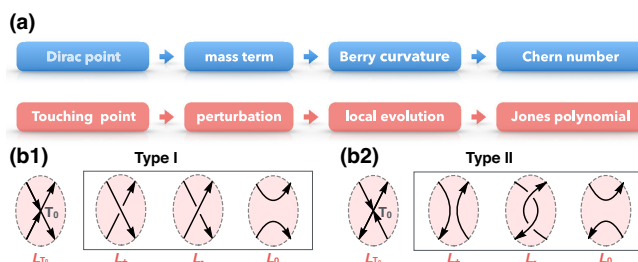

FIG. 1. The global topological invariants can be characterized by the local physics around some special points. The Chern insulators (nodal knot semimetals) can be viewed as generated phases from a critical phase with one or several Dirac points (TPs). The transition of Chern number (Jones polynomial) is attributed to the evolution changes of Berry curvature (local nodal lines) around the Dirac points (TPs) in the presence of perturba-tions. Panel (b) shows two possible line orientations (types I and II) around the TPs and the arrows indicate the directions of the nodal lines. There are three possible local evolutions for each line orientation.
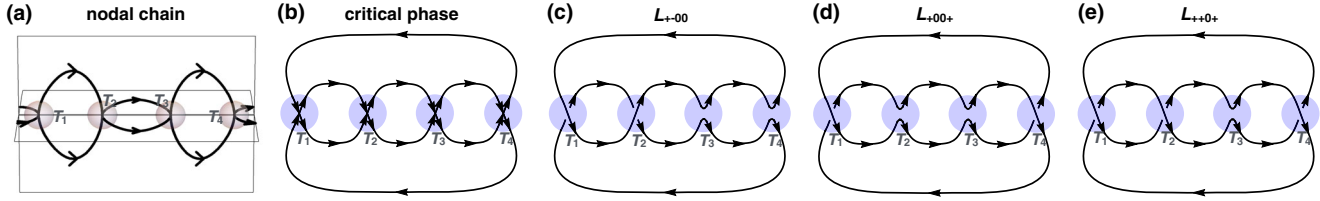
FIG. 2. Critical phase with TPs and generated phases without TPs. Panel (a) shows the nodal chain semimetal with 4 TPs. Panel (b) shows the critical phase, which is equivalent to (a) based on the periodic boundary condition of the 3D BZ. Panels (c)–(e) show several examples of the generated phases after the local evolutions of the 4 TPs.

polynomial can be analyzed by studying the local evolutions around all the TPs in a critical phase as shown in Fig. 1. In particular, the low energy theory of the TP provides additional constraints to the local evolutions and rules out the emergence of some generated phases. In the end, we extend the recipe of the knot topology analysis to non-Hermitian exceptional line semimetals [49,53–56,56–59], since Hermitian chiral symmetric systems and non-Hermitian systems share the identical mathematical structures.

Nodal line semimetals protected by chiral symmetry.— We start with a general $2N$-bands Bloch Hamiltonian preserving chiral symmetry

$$\mathcal{H}_0(\boldsymbol{k}) = h_0(\boldsymbol{k})\tau_+ + h_0^\dagger(\boldsymbol{k})\tau_-, \tag{1}$$

where $\tau_\pm = (\tau_x \pm i\tau_y)/2$, $h_0(\boldsymbol{k})$ is an $N \times N$ matrix, and chiral symmetry operator $\mathcal{S} = \tau_z$. Due to chiral symmetry, the Hamiltonian obeys $\mathcal{S}\mathcal{H}_0(\boldsymbol{k})\mathcal{S}^{-1} = -\mathcal{H}_0(\boldsymbol{k})$ and the locations of the nodal lines at $E = 0$ are determined by

$$\det[h_0(\boldsymbol{k})] = \det[h_0^\dagger(\boldsymbol{k})]^* = \gamma_0^r(\boldsymbol{k}) + i\gamma_0^i(\boldsymbol{k}) = 0. \tag{2}$$

In other words, the two constraints of $\gamma_0^r(\boldsymbol{k}) = 0$ and $\gamma_0^i(\boldsymbol{k}) = 0$ determine two surfaces in the 3D BZ, respectively, so that their crossings form the nodal lines.

A local topological invariant characterizing each individual nodal line is given by the winding number [52]

$$\nu = \frac{i}{2\pi} \oint_{\Gamma(\boldsymbol{K_0})} d\boldsymbol{k} \cdot \nabla_{\boldsymbol{k}} (\ln \det[h_0(\boldsymbol{k})]), \tag{3}$$

where $\boldsymbol{K}_0$ is a point located at the nodal lines and $\Gamma(\boldsymbol{K}_0)$ is a small circle enclosing the nodal line and centered at $\boldsymbol{K}_0$. If the winding number is nonzero, the integral path is not contractible so that these nodal lines are topologically protected and can not be gapped in the presence of any weak chiral-symmetric perturbations. One can also assign an orientation to the nodal line which is given by the normal vector of the positive winding number integral path determined by the right-hand rule and centered at $\boldsymbol{K}_0$ [52].

Critical phase and generated phases.— Now we show that all the generated phases from a critical phase with perturbations can be classified by local evolutions around every TP. Consider a critical phase with m TPs, which can

be labeled by $L_{T_1,...,T_m}$. Particularly, we use $m = 4$ as an example [Fig. 2(a)] through this manuscript. By adding a general form of perturbation respecting chiral symmetry

$$\mathcal{H}_1(\boldsymbol{k}, \lambda) = \lambda h_1(\boldsymbol{k}, \lambda)\tau_+ + \lambda h_1^\dagger(\boldsymbol{k}, \lambda)\tau_-, \tag{4}$$

where λ is an external parameter, these TPs are removed. Since the perturbation is weak, only the local evolutions around the TPs finally determine the linking or knotting properties of the nodal lines. Let us take the critical phase in Fig. 2(a) as a concrete example. To systematically study the generated phases, we project the critical phase in the 3D BZ [Fig. 2(a)] into a 2D plane and deform the projection to the diagram in Fig. 2(b) based on the periodic boundary condition of the 3D BZ. According to the directions of the nodal lines near the TPs, there exist two different types of TPs and the corresponding local evolutions $L_{0/+/-}$, namely type I (type II) TP and type I (type II) local evolutions as shown in Fig. 1(b1) [Fig. 1(b2)] [52]. In this regard, the generated phases evolving from the critical phase (multiple TPs) can be labeled by $L_{n_1...n_m}$, where $n_i = 0, \pm$ represent the local evolutions near the ith TP T_i; Figs. 2(c)–2(e) show several possible generated phases. We note that $L_{n_1,...,n_m}$ are the 2D projection representation of the 3D knot, which is known as knot diagram [52]. Although different projection planes lead to distinct knot diagrams of the same knot, the invariant, which will be given later, is independent of the choice of the projection plane [50].

Jones polynomial.— Having obtained all the perturbation generated phases, we define the corresponding knot invariant to characterize them. In knot theory, the topology of inequivalent knots can be distinguished by distinct knot polynomials [50]. We specifically use the Jone polynomial $J(L_\#)$ to characterize knots $L_\#$ in the nodal line semimetals, since the Jones polynomial can distinguish the orientations of the knots [60] from the directions of the winding numbers as well as reveals that the knot topology connects potential physical observables by using Chern-Simons theory [46,61,62]. On the one hand, since the Jones polynomial is a knot invariant, any two equivalent orientated knots must have the same Jones polynomial. On the other hand, the Jones polynomial for any given orientated knot can be calculated from the skein relation [50],

TABLE I. The Jones polynomials represent all the generated phases $L_{n_1 n_2 n_3 n_4}$ evolving from the nodal chain in Fig. 2(a), where $n_i = 0, \pm 1$. As $\vec{\nabla}_k \det[h_0(\mathbf{k})] \neq 0$ each TP, the evolution is limited to the unknot, unlink and Hopf link.

Links or knots	Jones polynomial	$n = \sum_{i=1}^4 n_i$
Unknot	1	$|n| = 1$
Unlink	$-t^{-1/2} - t^{1/2}$	$|n| = 0$
Hopf link	$-t^{5\text{sign}(n)/2} - t^{\text{sign}(n)/2}$	$|n| = 2$
Trefoil knot	$-t^{4\text{sign}(n)} + t^{3\text{sign}(n)} + t^{\text{sign}(n)}$	$|n| = 3$
Solomon's knot	$-t^{9\text{sign}(n)/2} - t^{5\text{sign}(n)/2}$	$|n| = 4$
	$+ t^{3\text{sign}(n)/2} - t^{\text{sign}(n)/2}$	

$$t^{-1}J(L_+) - tJ(L_-) + (t^{-1/2} - t^{1/2})J(L_0) = 0, \quad (5)$$

where L_+, L_- and L_0 are the Jones polynomials of three oriented knots having the only difference in the small red region as shown in Fig. 1(b1). Specifically, by labeling an unknot (ring) with O, its Jones polynomial is given by $J(O) \equiv 1$ as the starting point. By using this initial Jones polynomial and the skein relation, we provide a simple example to obtain the Jones polynomial of the unlink (two separate loops). Evaluating the local evolution around T_4 in Fig. 2(c), we obtain, $t^{-1}J(L_{+-0+}) - tJ(L_{+-0-}) + (t^{-1/2} - t^{1/2})J(L_{+-00}) = 0$. It can be checked that L_{+-0+} and L_{+-0-} are unknot [52], which implies $J(L_{+-0+}) = J(L_{+-0-}) = 1$. Solving the skien relation, we finally obtain $J(L_{+-00}) = -t^{-1/2} - t^{1/2}$ for the unlink. We note that the standard skein relation only connects the Jones polynomials of the generated phases around type I TP. In order to relate the Jones polynomials of all the generated phases including the type II local evolution, we extend the skein relation from type I to type II [Fig. 2(b2)] [52]. Therefore, any given $J(L_{n_1,...,n_m})$ can be calculated systematically via the skein relation and the initial condition $J(O) = 1$.

To demonstrate the approach of obtaining the explicit form of the Jones polynomial, we consider the evolution of the nodal chains with 4 TPs in the semimetals as shown in Fig. 2(a). Due to the orientations of the nodal lines, each local evolution near the TP can transit to three configurations L_+, L_- and L_0 of type I in Fig. 1(b1). First, knowing the Jones polynomials of the unlink and the unknot, we have $J(L_{+00-}) = -t^{-1/2} - t^{1/2}$ and $J(L_{+000}) = 1$ and then obtain the polynomial of the Hopf link $J(L_{+00+}) = -t^{5/2} - t^{1/2}$ by the skein relation at T_4 as illustrated in Fig. 2(d). Second, the skein relation at T_2 also connects an unknot L_{+-0+}, a Hopf link L_{+00+}, and a trefoil knot L_{++0+} as shown in Fig. 2(e); hence, the trefoil knot invariant is given by $J(L_{++0+}) = -t^4 + t^3 + t$. By following these rules, we can have the Jones polynomials for the 3^4 configurations of $L_{n_1 n_2 n_3 n_4}$ listed in Table I. In this model, the topology of the generated phases can be simply determined by the summation of the local diagram around every TP, which

$T(k_0)=0$	$\gamma_0^r(k)=\gamma_0^i(k)=0$	TP	Possible evolutions
Case (i) Linear Linear		Type II	
Case (ii) Linear Quadratic		Type II	
Case (iii) Quadratic Quadratic		Type I	

FIG. 3. The classification of the local evolution of two nodal lines with a single TP in the viewpoint of the *natural projective plane*, which is the plane spanned by the two tangential vectors at the TP of the two nodal lines. The first column shows the low energy theory around TP can be linear (nonvanishing gradient) or quadratic (vanishing gradient) in different cases. Here linear means linear dispersion of γ_0^r or γ_0^i along one direction in the BZ. This limits the possible geometry forms of the surface $\gamma_0^{r/i}(\mathbf{k}) = 0$ as shown in the second column. The third column shows the possible local evolutions under the constraint low energy theory of TP.

is similar to the transition of Chern number as shown in Fig. 1(a). It is not difficult to extend our analysis to the Jones polynomial of any generic critical phase with several TPs by using the iterations of the skein relation. Only the local evolution around the TP plays an essential role in determining the topology of generated phases.

Physical constraint.—We show that not only the orientations of the nodal lines but also the energy dispersions limit the possibilities of the local evolutions near the TPs. To show the limitation from the dispersions, we first study the conditions for the emergence of TPs in the Hamiltonian (1). Mathematically, these TPs are considered as singularity points of the nodal lines [52], which are defined by the vanishing of the tangent vector along the nodal lines at the points. Since the nodal line is located at the intersection of two surfaces $\gamma_0^r(\mathbf{k}) = 0$ and $\gamma_0^i(\mathbf{k}) = 0$, for a point $\mathbf{k}_0$ on the nodal line, the tangent vector $\mathbf{T}(\mathbf{k}_0)$ is perpendicular to the two normal directions $\vec{\nabla}_k \gamma_0^r(\mathbf{k}_0)$ and $\vec{\nabla}_k \gamma_0^i(\mathbf{k}_0)$, where $\vec{\nabla}_k = (\partial_{k_x}, \partial_{k_y}, \partial_{k_z})$. Therefore, the tangent vector at point $\mathbf{k}_0$ along the nodal line is given by

$$\mathbf{T}(\mathbf{k}_0) = \vec{\nabla}_k \gamma_0^r(\mathbf{k}_0) \times \vec{\nabla}_k \gamma_0^i(\mathbf{k}_0). \quad (6)$$

Since the TP in the nodal line belongs to a singularity point, the momentum $\mathbf{k}_{\text{TP}}$ at the TP obeys $\gamma_0^r(\mathbf{k}_{\text{TP}}) = \gamma_0^i(\mathbf{k}_{\text{TP}}) = \mathbf{T}(\mathbf{k}_{\text{TP}}) = 0$. To have $\mathbf{T}(\mathbf{k}_{\text{TP}}) = 0$, the TP evolution is classified as the three cases: (i) the two gradients are parallel $[\vec{\nabla}_k \gamma_0^r(\mathbf{k}_{\text{TP}}) = c\vec{\nabla}_k \gamma_0^i(\mathbf{k}_{\text{TP}}) \neq 0]$, (ii) one of the gradients vanishes, and (iii) both vanish as shown in Fig. 3. In particular, for cases (i) and (ii), at least one of the two surfaces must have nonzero gradients at $\mathbf{k}_{\text{TP}}$, which satisfies $\vec{\nabla}_k \det[h_0(\mathbf{k}_{\text{TP}})] \neq 0$. Since local evolutions are different in
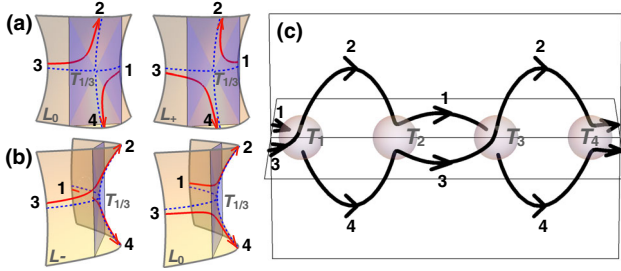
FIG. 4. Hopf-link semimetal. Panel (a) shows the physical constraint to the local evolutions of the TPs $T_{1/3}$. Only $L_{0/+}$ of type II are possible in the natural projective plane (blue plane). However, if we rotate the figures in (a), the local evolution becomes $L_{-/0}$ of type I as shown in (b). Panel (c) shows the Hopf-link semimetal can be obtained from the model in Fig. 2(a) by adding the perturbation $\lambda h_1(\boldsymbol{k}, \lambda) = i\lambda \sin 2k_x$.

different projective planes, we specifically choose the natural projective plane, which is spanned by the two tangential vectors at the TP. For cases (i) and (ii), the natural projective plane is perpendicular to the normal vector $\vec{\nabla}_k \gamma_0^{r/i}(\boldsymbol{k}_{\mathrm{TP}})$. It can be shown that for the first two cases the TP must be type II in the natural projective plane [52], and the local evolution near the TP is limited to the two possibilities shown in the first two rows of Fig. 3. The reason is that the surface with nonzero gradient at the TP (yellow surface) can always be mapped to the natural projective plane (light blue plane) as shown in Fig. 4(a). The spatial limitation forbids the emergence of L_- in Fig. 1(b2). Here we emphasize that the limitation of the local evolution holds only in the *natural projective planes*. Choosing another projective plane, we have to transfer the constraint from the natural projective plane to the chosen plane. For example, Fig. 4(a) shows only L_+ and L_0 of type II are the only two possible local evolutions in the natural projective plane. By changing a projective view and applying this evolution constraint, Fig. 4(b) in the new projective plane shows that the two possible local evolutions become L_- and L_0 of type I in Fig. 1(b1).

On the other hand, in case (iii) neither $\gamma_0^r(\boldsymbol{k})$ nor $\gamma_0^i(\boldsymbol{k})$ possesses linear terms near $\boldsymbol{k}_{\mathrm{TP}}$ as shown in the third row of Fig. 3. By assuming quadratic terms of $\boldsymbol{k}$, in the *natural projective plane*, the line arrangement at the TP is constrained to type I, and there are three possible evolutions as shown in Fig. 3 [52].

Nodal chain semimetals.—To demonstrate the tools we established for the study of the knot evolution in semimetals, we are back to the nodal chain semimetal with 4 TPs protected by chiral and two mirror symmetries [6,23]. We consider a specific nodal chain described by the chiral symmetric Hamiltonian (1) with $h_0(\boldsymbol{k}) = 2\cos 2k_x + \cos k_x + 3\cos k_y - 3\cos k_z - 1/10 - 2i\sin k_y \sin k_z$ as shown in Fig. 2(a) [52]. In this model, $\vec{\nabla}_k \det[h_0(\boldsymbol{k}_{\mathrm{TP}})] \neq 0$ [6]. First, consider the local evolutions at T_1, T_3, which can

have only L_+ and L_0 of type II in the natural projective planes (blue planes) as shown in Fig. 4(a). In the other view angle for the knot diagrams in Figs. 2(b)–2(d), L_- and L_0 of type I are only two possible evolutions as shown in Fig. 4(b). Similarly, the TPs T_2, T_4 in the projective planes can evolve only to L_+ and L_0 of type I in the knot diagram. Consequently, the generated phases are constrained to be $L_{n_1 m_1 n_2 m_2}$, where $n_i = 0$, 1 and $m_i = 0, -1$. Due to this constraint from the linear dispersion, globally the chain can evolve to an unknot ($|n| = 1$), an unlink ($|n| = 0$), or a Hopf link ($|n| = 2$) listed in Table I. As shown in Fig. 4(c), we have a nodal Hopf link under the perturbation Eq. (4) with $\lambda h_1(\boldsymbol{k}, \lambda) = i\lambda \sin 2k_x$. Physically, we have two ways to control perturbations. One is to add the pressure of a material that breaks the mirror symmetry. The other way is that in the photonic lattice, the lattice can be designed artificially. Hence the mirror symmetry breaking term can be added in a controlled way [63]. Finally, using the same recipe, we can show that the nodal chain semimetal ($L_{n_1 m_1}$) with 2 TPs cannot evolve to a Hopf link ($L_{\pm\pm}$) when $\vec{\nabla}_k \det[h_0(\boldsymbol{k}_{\mathrm{TP}})] \neq 0$ at each TP [52].

Non-Hermitian exceptional line semimetals.—This recipe studying the knot topology can even be extended to the non-Hermitian system [64–73], namely, the 3D non-Hermitian exceptional line semimetals [49,53–56,56–59]. While in Hermitian systems the nodal lines require symmetry protection [6], the non-Hermitian exceptional lines are robust against any small perturbation even in the absence of any symmetries [49,69]. We here focus on general N-band non-Hermitian Bloch Hamiltonians $\mathcal{H}_{nH}(\boldsymbol{k})$ [70–76]. According to the characteristic polynomial of the Hamiltonian $f(E, \boldsymbol{k}) = \det[E - \mathcal{H}_{nH}(\boldsymbol{k})] = \Pi_{i=1}^N [E - E_i(\boldsymbol{k})]$, the condition for the emergence of band degeneracy $E_i(\boldsymbol{k}) = E_j(\boldsymbol{k})$ requires [52,77]

$$\Delta_f(\boldsymbol{k}) = \prod_{i<j} [E_i(\boldsymbol{k}) - E_j(\boldsymbol{k})]^2 = 0, \qquad (7)$$

where $\Delta_f(\boldsymbol{k})$ is the discriminant of the characteristic polynomial $f(E, \boldsymbol{k})$ as a function of E [52]. For example, if $f(E) = aE^2 + bE + c$, $\Delta_f = b^2 - 4ac$. Hence, the solution of Eq. (7) must be a set of 1D degeneracy lines in the 3D BZ. Using the Sylvester matrix of the characteristic polynomial to build the discriminant [52,77–79], we can show the discriminant is a single-valued function of $\boldsymbol{k}$. Therefore, the topological charge can be defined by the quantized winding number in Eq. (3) with $h_0(\boldsymbol{k}) = \Delta_f(\boldsymbol{k})$, and the nonzero winding number protects the degeneracy line and determines the knot orientation. Since the mathematical structures of the Hermitian chiral symmetric systems and non-Hermitian ones are identical, the aforementioned recipe can be extended to non-Hermitian systems.

In summary, topologically protected lines emerge in distinct condensed matter systems, such as Hermitian

chiral-symmetric semimetals and non-Hermitian systems. We start with nodal lines with several TPs; the Jones polynomial characterizes the knot topology of the lines with orientation in 3D BZ, and the topology essentially is only determined by the local evolution near each TP. The low energy theory limits the line orientation at any TP; furthermore, if $\vec{\nabla}_{\boldsymbol{k}} \det[h_0(\boldsymbol{k}_{\mathrm{TP}})]$ in the Hermitian semimetals or $\vec{\nabla}_{\boldsymbol{k}} \Delta_f(\boldsymbol{k}_{\mathrm{TP}})$ in the non-Hermitian systems does not vanish at the TP, the corresponding local evolution is limited to two possible ones. Our methodology provides general rules to the evolution of the topologically protected lines with TPs and paves the way toward searching for exotic topological nodal knot semimetals.

*qiujingkai@ucas.edu.cn
†cfang@iphy.ac.cn
‡jphu@iphy.ac.cn

[1] M. Z. Hasan and C. L. Kane, Rev. Mod. Phys. **82,** 3045 (2010).

[2] X.-L. Qi and S.-C. Zhang, Rev. Mod. Phys. **83,** 1057 (2011).

[3] A. Bansil, H. Lin, and T. Das, Rev. Mod. Phys. **88,** 021004 (2016).

[4] C.-K. Chiu, J. C. Y. Teo, A. P. Schnyder, and S. Ryu, Rev. Mod. Phys. **88,** 035005 (2016).

[5] N. P. Armitage, E. J. Mele, and A. Vishwanath, Rev. Mod. Phys. **90,** 015001 (2018).

[6] C. Fang, H. Weng, X. Dai, and Z. Fang, Chin. Phys. B **25,** 117106 (2016).

[7] A. B. Bernevig and T. L. Hughes, *Topological Insulators and Topological Superconductors* (Princeton University Press, Princeton, NJ, 2013).

[8] T. Hughes, Time-reversal invariant topological insulators, Ph. D. Thesis, Stanford University, 2009.

[9] B. A. Bernevig, T. L. Hughes, and S.-C. Zhang, Science **314,** 1757 (2006).

[10] C.-K. Chiu, arXiv:1410.1117.

[11] P. Hořava, Phys. Rev. Lett. **95,** 016405 (2005).

[12] A. A. Burkov, M. D. Hook, and L. Balents, Phys. Rev. B **84,** 235126 (2011).

[13] Y. Chen, Y.-M. Lu, and H.-Y. Kee, Nat. Commun. **6,** 6593 (2015).

[14] Y. Kim, B. J. Wieder, C. L. Kane, and A. M. Rappe, Phys. Rev. Lett. **115,** 036806 (2015).

[15] K. Mullen, B. Uchoa, and D. T. Glatzhofer, Phys. Rev. Lett. **115,** 026403 (2015).

[16] R. Yu, H. Weng, Z. Fang, X. Dai, and X. Hu, Phys. Rev. Lett. **115,** 036807 (2015).

[17] C. Fang, Y. Chen, H.-Y. Kee, and L. Fu, Phys. Rev. B **92,** 081201(R) (2015).

[18] G. Bian *et al.*, Nat. Commun. **7,** 10556 (2016).

[19] Y.-H. Chan, C.-K. Chiu, M. Y. Chou, and A. P. Schnyder, Phys. Rev. B **93,** 205132 (2016).

[20] L. M. Schoop, M. N. Ali, C. Straßer, A. Topp, A. Varykhalov, D. Marchenko, V. Duppel, S. S. P. Parkin, B. V. Lotsch, and C. R. Ast, Nat. Commun. **7,** 11696 (2016).

[21] T. Bzdušek, Q. Wu, A. Rüegg, M. Sigrist, and A. A. Soluyanov, Nature (London) **538,** 75 (2016).

[22] R. Yu, Q. Wu, Z. Fang, and H. Weng, Phys. Rev. Lett. **119,** 036401 (2017).

[23] Q. Yan, R. Liu, Z. Yan, B. Liu, H. Chen, Z. Wang, and L. Lu, Nat. Phys. **14,** 461 (2018).

[24] X. Feng, C. Yue, Z. Song, Q. S. Wu, and B. Wen, Phys. Rev. Mater. **2,** 014202 (2018).

[25] C. Gong, Y. Xie, Y. Chen, H.-S. Kim, and D. Vanderbilt, Phys. Rev. Lett. **120,** 106403 (2018).

[26] Z. Liu, R. Lou, P. Guo, Q. Wang, S. Sun, C. Li, S. Thirupathaiah, A. Fedorov, D. Shen, K. Liu, H. Lei, and S. Wang, Phys. Rev. X **8,** 031044 (2018).

[27] D.-F. Shao, S.-H. Zhang, X. Dang, and E. Y. Tsymbal, Phys. Rev. B **98,** 161104(R) (2018).

[28] R. Lou, P. Guo, M. Li, Q. Wang, Z. Liu, S. Sun, C. Li, X. Wu, Z. Wang, Z. Sun, D. Shen, Y. Huang, K. Liu, Z.-Y. Lu, H. Lei, H. Ding, and S. Wang, npj Quantum Mater. **3,** 43 (2018).

[29] C.-J. Yi, B. Q. Lv, Q. S. Wu, B.-B. Fu, X. Gao, M. Yang, X.-L. Peng, M. Li, Y.-B. Huang, P. Richard, M. Shi, G. Li, O. V. Yazyev, Y.-G. Shi, T. Qian, and H. Ding, Phys. Rev. B **97,** 201107(R) (2018).

[30] B. Fu, X. Fan, D. Ma, C.-C. Liu, and Y. Yao, Phys. Rev. B **98,** 075146 (2018).

[31] B. Singh, S. Mardanya, C. Su, H. Lin, A. Agarwal, and A. Bansil, Phys. Rev. B **98,** 085122 (2018).

[32] Q. Wu, A. A. Soluyanov, and T. Bzdušek, Science **365,** 1273 (2019).

[33] R. Kim, B.-J. Yang, and C. H. Kim, Phys. Rev. B **99,** 045130 (2019).

[34] C. Chen, Z.-M. Yu, S. Li, Z. Chen, X.-L. Sheng, and S. A. Yang, Phys. Rev. B **99,** 075131 (2019).

[35] J. Lian, L. Yu, Q.-F. Liang, J. Zhou, R. Yu, and H. Weng, npj Comput. Mater. **5,** 10 (2019).

[36] W. Chen, H.-Z. Lu, and J.-M. Hou, Phys. Rev. B **96,** 041102 (R) (2017).

[37] Z. Yan, R. Bi, H. Shen, L. Lu, S.-C. Zhang, and Z. Wang, Phys. Rev. B **96,** 041103(R) (2017).

[38] P.-Y. Chang and C.-H. Yee, Phys. Rev. B **96,** 081114(R) (2017).

[39] Y. Zhou, F. Xiong, X. Wan, and J. An, Phys. Rev. B **97,** 155140 (2018).

[40] Y. Wang, H. Hu, and S. Chen, Phys. Rev. B **98,** 205410 (2018).

[41] G. Chang, S.-Y. Xu, X. Zhou, S.-M. Huang, B. Singh, B. Wang, I. Belopolski, J. Yin, S. Zhang, A. Bansil, H. Lin, and M. Z. Hasan, Phys. Rev. Lett. **119,** 156401 (2017).

[42] X.-Q. Sun, B. Lian, and S.-C. Zhang, Phys. Rev. Lett. **119,** 147001 (2017).

[43] L. Li, C. H. Lee, and J. Gong, Phys. Rev. Lett. **121,** 036401 (2018).

[44] M. Ezawa, Phys. Rev. B **96,** 041202(R) (2017).

[45] R. Bi, Z. Yan, L. Lu, and Z. Wang, Phys. Rev. B **96,** 201305 (R) (2017).

[46] B. Lian, C. Vafa, F. Vafa, and S.-C. Zhang, Phys. Rev. B **95,** 094512 (2017).

[47] T. Bzdušek and M. Sigrist, Phys. Rev. B **96,** 155105(R) (2017).

[48] A. Tiwari and T. Bzdušek, arXiv:1903.00018.

[49] Z. Yang and J. Hu, Phys. Rev. B **99,** 081102(R) (2019).

[50] L. H. Kauffman, Knots and Physics (World Scientific, Singapore, 1991).

[51] R. Hepworth, Mx4540: Knots, https://homepages.abdn.ac .uk/r.hepworth/pages/.

[52] See the Supplemental Material at http://link.aps.org/ supplemental/10.1103/PhysRevLett.124.186402 for more details, which includes the following: (i) derivation of the winding number of nodal lines protected by chiral symmetry and the corresponding definition of orientations, (ii) introduction of knot theory and Jones polynomial, (iii) classification of local evolutions, (iv) extended skien relations, (v) introduction of singularity points, (vi) physical constraint of local evolutions, (vii) nodal chain semimetals protected by two mirror symmetries, and (viii) introduction of discriminant.

[53] Y. Xu, S.-T. Wang, and L.-M. Duan, Phys. Rev. Lett. **118,** 045701 (2017).

[54] A. Cerjan, M. Xiao, L. Yuan, and S. Fan, Phys. Rev. B **97,** 075128 (2018).

[55] J. Carlström and E. J. Bergholtz, Phys. Rev. A **98,** 042114 (2018).

[56] J. Carlström, M. Stålhammar, J. C. Budich, and E. J. Bergholtz, Phys. Rev. B **99,** 161115(R) (2019).

[57] K. Moors, A. A. Zyuzin, A. Y. Zyuzin, R. P. Tiwari, and T. L. Schmidt, Phys. Rev. B **99,** 041116(R) (2019).

[58] H. Wang, J. Ruan, and H. Zhang, Phys. Rev. B **99,** 075130 (2019).

[59] K. Kawabata, T. Bessho, and M. Sato, Phys. Rev. Lett. **123,** 066405 (2019).

[60] V. F. R. Jones, Bull. Am. Math. Soc. **12,** 103 (1985).

[61] E. Witten, Commun. Math. Phys. **121,** 351 (1989).

[62] J. Fröhlich and C. King, Commun. Math. Phys. **126,** 167 (1989).

[63] L. Lu, Z. Wang, D. Ye, L. Ran, L. Fu, J. D. Joannopoulos, and M. Soljačić, Science **349,** 622 (2015).

[64] C. M. Bender, Rep. Prog. Phys. **70,** 947 (2007).

[65] L. Feng, R. El-Ganainy, and L. Ge, Nat. Photonics **11,** 752 (2017).

[66] R. El-Ganainy, K. G. Makris, M. Khajavikhan, Z. H. Musslimani, S. Rotter, and D. N. Christodoulides, Nat. Phys. **14,** 11 (2018).

[67] Ş. K. Özdemir, S. Rotter, F. Nori, and L. Yang, Nat. Mater. **18,** 783 (2019).

[68] M.-A. Miri and A. Alù, Science **363,** eaar7709 (2019).

[69] H. Shen, B. Zhen, and L. Fu, Phys. Rev. Lett. **120,** 146402 (2018).

[70] S. Yao and Z. Wang, Phys. Rev. Lett. **121,** 086803 (2018).

[71] S. Yao, F. Song, and Z. Wang, Phys. Rev. Lett. **121,** 136802 (2018).

[72] K. Yokomizo and S. Murakami, Phys. Rev. Lett. **123,** 066404 (2019).

[73] K. Zhang, Z. Yang, and C. Fang, arXiv:1910.01131.

[74] F. Song, S. Yao, and Z. Wang, Phys. Rev. Lett. **123,** 170401 (2019).

[75] N. Okuma, K. Kawabata, K. Shiozaki, and M. Sato, Phys. Rev. Lett. **124,** 086801 (2020).

[76] Z. Yang, K. Zhang, C. Fang, and J. Hu, arXiv:1912.05499.

[77] Z. Yang, A. P. Schnyder, J. Hu, and C.-K. Chiu, arXiv: 1912.02788.

[78] H. Woody, Polynomial resultants, http://buzzard.ups.edu/ courses/2016spring/projects/woody-resultants-ups-434-2016.pdf.

[79] S. Janson, Resultant and discriminant of polynomials (2010), http://www2.math.uu.se/~svante/papers/sjN5.pdf.